



# Reactivity of an Air-Stable Dihydrobenzoimidazole n-Dopant with Organic Semiconductor Molecules

Samik Jhulki,<sup>1</sup> Hio-leng Un,<sup>1,2</sup> Yi-Fan Ding,<sup>2</sup> Chad Risko,<sup>3</sup> Swagat K. Mohapatra,<sup>1,4</sup> Jian Pei,<sup>2,\*</sup> Stephen Barlow<sup>1,5\*\*</sup>, Seth R. Marder<sup>1,\*\*\*</sup>

<sup>1</sup>School of Chemistry and Biochemistry and Center for Organic Photonics and Electronics, Georgia Institute of Technology, Atlanta, GA 30332-0400, USA <sup>2</sup>Beijing National Laboratory for Molecular Sciences (BNLMS), Key Laboratory of Polymer Chemistry and Physics of Ministry of Education, Center of Soft Matter Science and Engineering, and College of Chemistry and Molecular Engineering, Peking University, Beijing 100871, China <sup>3</sup>Department of Chemistry & Center for Applied Energy Research (CAER), University of Kentucky, 2582 Research Park Drive, Lexington, Kentucky 40511, USA

Department of Industrial and Engineering Chemistry, Institute of Chemical Technology – Indian Oil Odisha Campus, Bhubaneswar, Odisha 751013, India

SLead Contact

#### **SUMMARY**

1,3-Dimethyl-2-(4-(dimethylamino)phenyl)-2,4-dihydro-1*H*-benzoimidazole, N-DMBI-H, is widely used as an air-stable n-dopant for organic semiconductors. Here its reactivity is investigated with a variety of imide- and amide-containing semiconductor molecules with reduction potentials in the range –0.54 to –1.10 V vs. ferrocene. Reaction rates correlate poorly with these potentials. The more reactive of the imides form the corresponding radical anions cleanly, but kinetic isotope studies using N-DMBI-D indicate that the reaction proceeds via an initial hydride- or hydrogen-transfer step. For an amide- and ester-rigidified bis(styryl)benzene derivative the hydride-reduced product is stable under inert atmosphere and can be observed directly; the radical anion can only be obtained in sub-stoichiometric yield and under certain reaction conditions. On the other hand, (N-DMBI)<sub>2</sub> rapidly reduces all the imides and amides examined to the corresponding radical anions. The implications of these findings for dopant selection and use are discussed.

Keywords: dopant, hydride transfer, benzoimidazole, mechanism, kinetic isotope effect

<sup>\*</sup>Correspondence: jianpei@pku.edu.cn

<sup>\*\*</sup>Correspondence: stephen.barlow@chemistry.gatech.edu

<sup>\*\*\*</sup>Correspondence: seth.marder@chemistry.gatech.edu

# Cell<sup>2</sup>ress



#### INTRODUCTION

Electrical doping of organic semiconductors using molecular oxidants or reductants can be used to increase electrical conductivity and to facilitate charge-carrier injection and, accordingly, can play important roles in a variety of established and emerging applications. 1-4 The simplest approach to n-doping (reduction) is through dopant-to-semiconductor electron transfer (ET), which, to achieve a high doping efficiency, i.e. a high yield of charge carriers with respect to dopant molecules, should be exergonic. For efficient n-doping via ET of even materials with moderate electron affinity, such as fullerenes, suitable dopants, such as cobaltocene,<sup>5</sup> have low ionization energies and are consequently sensitive to ambient conditions, complicating their storage and use. To obtain adequately reducing yet relatively airstable n-dopants, several classes of n-dopants have been identified and/or developed in which ET reactions are coupled with other chemical reactions. One such class are organic hydride donors such as leuco crystal violet<sup>6</sup> and 1,3-dialkyl-2,3-dihydro-1*H*-benzoimidazole derivatives (Y-DMBI-H, **IH**, Figure 1).<sup>7</sup> Due to their air stability and straightforward synthesis, 8-10 Y-DMBI-H derivatives have been increasingly used in recent years, both for the n-doping of many organic semiconductors for various applications, 11-19 and for surface n-doping of materials such as graphene, 20 carbon nanotubes, 21 and few-layer MoS<sub>2</sub>. 22 A variety of IH derivatives have been used, including dopants developed: to tune the reactivity with acceptors;<sup>23-25</sup> to increase air stability in solution;<sup>26</sup> and for improved miscibility with, 16,27 or covalent attachment to, 28 semiconductors. However, the most widely used is 1,3-dimethyl-2-(4-(dimethylamino)phenyl)-2,3-dihydro-1H-benzoimidazole, N-DMBI-H (IaH, Figure 1). Although high electrical conductivities have been obtained with some semiconductors, 14,17-19 low doping efficiencies or phase separation of the dopant, suggesting incomplete reaction, are found in others, 13,16 at least without thermal annealing. Therefore, an understanding of the mechanism by which IaH reacts with different semiconductors is needed to rationalize these findings and help guide its future use.

The mechanism of the solution reaction of **IaH** and the fullerene derivative PCBM (**1**, Figure 1) has been investigated.<sup>29</sup> Comparison of reaction rates using **IaH** and N-DMBI-D (**IaD**) reveals a primary kinetic isotope effect (KIE), indicating C-H bond cleavage to be the rate-determining step (RDS); the substituent dependence of reaction rates observed using a variety of different **IH** derivatives strongly suggest that this is a hydride-transfer reaction:

$$N-DMBI-H + PCBM \rightarrow N-DMBI^{+} + PCBMH^{-}$$
 (1)

In addition to the desired radical PCBM\*- (1\*-) and the expected N-DMBI+ (la\*), partially hydrogenated fullerene was also detected, suggesting rapid ET from PCBMH- to PCBM follows the H- transfer, so that the overall reaction is:

N-DMBI-H + 
$$(1+1/x)$$
PCBM  $\rightarrow$  N-DMBI+ + PCBM+- +  $(1/x)$ PCBMH<sub>x</sub> (2)

Thus, the thermodynamics of the overall doping reaction depend on both the electron- and hydrogen-accepting properties of the fullerene, and the kinetics depend on its hydride-accepting properties. Thus, in contrast to doping using simple ET reductants, such as cobaltocene, the thermodynamic and kinetic feasibility of doping via this reaction mechanism cannot be predicted based solely on the reduction potential of the acceptor,  $E^{0,\bullet}$ -(A). Furthermore, different acceptors could potentially react through different reaction pathways and form different side products. A more thorough and general understanding of the reaction mechanism(s) by which **laH** reacts with semiconductor molecules is needed to (i) gain insight into



the types of semiconductors to which this n-dopant can be usefully applied, (ii) help predict the timescales required for complete doping of different semiconductors, and (iii) inform the rational development of new n-dopants with improved properties.

Here we investigate the solution reactivity of **IaH** with a variety of amide- and imide-based acceptors (A) for which  $E^{0/*-}$  is close to, or more cathodic than the corresponding value for PCBM (Figure 1). First we present electrochemical and computational data pertaining to the electron-, hydrogen-atom-, and hydride-accepting abilities of the acceptors studied. Dimeric dopants – (RuCp\*mes)<sub>2</sub>, (**II**)<sub>2</sub>, and the recently reported dimeric analogue of **IaH**, (N-DMBI)<sub>2</sub>, (**Ia**)<sub>2</sub><sup>17</sup> – are used to generate reference solutions of the relevant A\*- species. The rates of reaction between the acceptors and **IaH** are discussed, followed by the effects of using **IaD** on these rates. We show, how, in contrast to most acceptors examined, which form A\*-, 2CN-BDPOV (**2**) is reduced to a remarkably stable AH<sup>-</sup> derivative that is only converted to A\*- under certain conditions. Aspects of the reaction mechanisms associated with **IaH** reductions are discussed. Finally, the implications of our findings for the selection of dopants and doping conditions are discussed.

#### **RESULTS**

#### **Acceptors and Dopants Under Consideration**

We focus on the reactivity of N-DMBI-H, IaH, with different classes of amide- and imide-based molecules (see Supplemental Information for synthetic details and Figures S1-S7 for characterization of 2). Both small molecules and more elaborate structures incorporating the same acceptor moieties, such as the conjugated polymers FBDPPV and P(NDI2OD-T2) (Figure 1), are widely studied as electrontransport materials for a wide range of applications.<sup>30</sup> The acceptors chosen thus represent classes of materials that researchers are interested in n-doping. The naphthalene and perylene diimides, 3a-c and 4a-c respectively, were chosen to enable the impact of their reduction potentials,  $E^{0,\bullet}(A)$ , on doping rates to be systematically investigated, these values ranging over almost 0.6 V (-0.54 to -1.10 V vs. FeCp<sub>2</sub><sup>+/0</sup>, Table 1, Figure S8). 2CN-BDOPV, **2**, can be regarded as an oligophenylenevinylene rigidified with electron-withdrawing ester and amide groups and as being an "expanded isoindigo", in which a dilactone-fused benzene bridge is present between the two oxoindoline units. It was specifically chosen (i) as an easily reduced semiconductor with similar  $E^{0/\bullet-}$  to the most readily reduced of the rylene diimides, 3b, and (ii) as a molecular model compound for polymers containing the same rigidified phenylenevinylene structural motifs, particularly FBDPPV,<sup>31</sup> which exhibits high conductivity values when doped by **IaH**.<sup>14,17</sup> Figure 1 also shows PCBM, 1, the reactivity of which with laH has previously been studied,29 and 6,13-bis(tri(isopropyl)silylethynyl)pentacene (TIPSp, 5).<sup>32</sup> 5 is less readily reduced (-1.45 V), typically functioning as a hole-transport material, 33 but has been rendered electron-transporting by IaH, 12 likely through trap-filling effects, 29 and has been used in our previous mechanistic work on dimeric n-dopants. 34,35

In principle, the reaction of IaH with a given A could proceed by an initial ET,

$$N-DMBI-H + A \rightarrow N-DMBI-H^{\bullet+} + A^{\bullet-}$$
(3)

followed by further reaction of  $IaH^{**}$  (clearly unstable from the irreversible cyclic voltammogram of  $IaH^{29}$ ) to form  $Ia^*$ .  $E^{0/*-}(A)$  values (Table 1) allow us to estimate the free energy change,  $\Delta G^0$ , for the ET reaction (eq. 3) between IaH (irreversibly oxidized at -0.13 V) and A; these values are given in Table 1 alongside values from gas-phase and solvent dielectric (polarizable continuum model,  $CH_2CI_2$ ,  $\varepsilon=8.93$ )



density-functional theory (DFT) calculations at the M06/6-31G(d,p)/LANL2DZ level (see also Tables S1-S3 and Figures S9-S11 for additional DFT data for reactions of **IaH**, **(Ia)**<sub>2</sub>, and the acceptors). Note that the gas-phase DFT  $\Delta G^0_3$  values are much larger than those estimated electrochemically, although the trends in these two sets of data are in good qualitative agreement (Figure S10). Calculation of values of  $\Delta G^0_3$  using a dielectric continuum to simulate dichloromethane, however, leads to values in good quantitative agreement with the electrochemical values. The range of variation of the gas-phase DFT values is also larger than that in the electrochemical or solution DFT values.

Alternatively, the reactions might proceed by initial hydrogen-atom transfer:

$$N-DMBI-H + A \rightarrow N-DMBI^{\bullet} + AH^{\bullet}$$
 (4)

or (as previously seen for  $A = PCBM^{29}$ ) hydride transfer:

$$N-DMBI-H + A \rightarrow N-DMBI^{+} + AH^{-}$$
 (5)

followed by subsequent reaction of AH\* or AH\* to give A\*\*. Table 1 also gives DFT estimates of  $\Delta G^0$  for the H $^{\bullet}$  and H $^{-}$  transfers, eq. 4 and eq. 5 respectively, in the gas phase and in solvent. We exclude the previously suggested dissociation of laH to la and free H from consideration, as explained in the Discussion section. We note that (with the exception of  $C_{60}$ , used as a model for PCBM) multiple isomers are possible for both AH\* and AH\*; unless noted otherwise, the values given in Table 1 refer to the most stable isomer for each A (data for all isomers are given in Table S3, with structures in Figure S11).  $\Delta G^{0_4}$  and  $\Delta G^{0_5}$  values do not correlate particularly well with each other, or with  $\Delta G^{0}_{3}$  values (Figure S12). For example, **2** has similar electron-accepting ability to **3b**, but is a stronger H<sup>-</sup> acceptor, while **5** is the weakest electron acceptor but the second strongest H $^{\bullet}$  acceptor. The values of  $\Delta G^{0}_{4}$ , which apply to reactions in which no charged species are involved, are generally (with the exception of that for 4c) insensitive to the inclusion of solvent in the calculations. On the other hand, the reactions described by eq. 5, like those described by eq. 3, involve formation of pairs of ions; these ions are more strongly stabilized by the inclusion of solvent in the calculations than the neutral species, and so values of both  $\Delta G^{0}_{5}$  and  $\Delta G^{0}_{3}$  are calculated to be more exergonic by 200+ kJ mol<sup>-1</sup> in solvent than the gas-phase).

Finally, Figure 1 also shows the chemical structures of two dimeric n-dopants, (N-DMBI)<sub>2</sub>, (Ia)<sub>2</sub>, <sup>17</sup> and (RuCp\*mes)<sub>2</sub>, (II)<sub>2</sub>, <sup>36</sup> and the cations they form on oxidation; as described in the following section, these dimers were used to obtain reference vis-NIR spectra for A\*- species.

#### **Reaction of Acceptors with Dimeric Dopants**

Dopants formed by the dimerization of Y-DMBI radicals,  $(I)_2$ , <sup>35</sup> or of 19-electron sandwich compounds, such as  $(II)_2$ , <sup>34</sup> react cleanly with acceptors according to:

$$D_2 + 2A \rightarrow 2D^+ + 2A^{\bullet -}$$
 (6)

The overall effective reducing strength of these dimers is related to the reduction potential of the corresponding monomeric cation and the free energy of dissociation of the dimer,  $\Delta G_{\text{diss}}(D_2)$ , according to:

$$E(D^{+}/0.5D_{2}) = E(D^{+}/D^{\bullet}) + (0.5/F)\Delta G_{diss}(D_{2})$$
(7)



where F is the Faraday constant. For (II)<sub>2</sub>, we previously reported  $E(D^+/0.5D_2) = -2.10$  V based on  $E(D^+/D^\bullet) = -2.67$  V and a DFT-calculated  $\Delta G_{\rm diss}$  of +110 kJ mol<sup>-1</sup> at 298 K.<sup>34,37</sup> For (Ia)<sub>2</sub> we estimate  $E(D^+/0.5D_2) = -1.94$  V using  $E(D^+/D^\bullet) = -2.38$  V,<sup>17</sup> and a DFT  $\Delta G_{\rm diss}$  of +85 kJ mol<sup>-1</sup> at 298 K (Table S1). Thus, both dimers are thermodynamically capable of reducing all the acceptors used in this study. The kinetic feasibility of reducing the most challenging acceptor discussed here, **5**, has been previously demonstrated with a close analogue of (II)<sub>2</sub>.<sup>34</sup>

We first confirmed that (Ia)<sub>2</sub> behaves similarly to (II)<sub>2</sub> in reactions with 2, 3b, and 5 in chlorobenzene. In each case, vis-NIR spectra obtained using (Ia)<sub>2</sub> are almost identical to those obtained using (II)<sub>2</sub> (Figure S13 and S14). Spectra for the full set of amide and imide amide acceptors shown in Figure 1 were then acquired using 0.5 equiv. Ia<sub>2</sub> to serve as reference spectra for reaction products obtained using IaH (Figure S14). The spectra obtained on reduction of the 3 and 4 derivatives are qualitatively similar to those previously reported for radical anions for these classes of acceptor.<sup>38</sup> In the case of 2, we also confirmed that the putative radical anion generated on addition of (Ia)<sub>2</sub> was quantitatively re-converted to neutral 2 on addition of an oxidant (Figure S13C). ESR also indicated this reduction product of 2 to be a radical; furthermore, the observed hyperfine pattern was consistent with DFT calculations for 2<sup>--</sup> (see Figure S15, Table S4). With the exception of 5, for which the D<sub>2</sub>-to-A ET is most endergonic and, therefore, the reduction is relatively slow, these reactions were found to be complete by the time the first spectrum could be acquired (i.e., after 2-3 min).

#### Reaction of Acceptors with N-DMBI-H

Reactions of N-DMBI-H, **IaH**, and the various acceptors were carried out in a 1:1 ratio in chlorobenzene in the dark (see Figures 2, 3, S16, and S17 for representative spectra). For the **3** and **4** derivatives, new absorption features were observed to grow over time, with concomitant disappearance of those of the neutral molecules. By comparison to the doping experiments with (**II**)<sub>2</sub> described above, the new visible signals could be ascribed to A\*- and a peak at 355 nm to **Ia**\*. However, the rates of appearance of these features were considerably slower than when doping with (**Ia**)<sub>2</sub> and varied considerably between acceptors. In the case of **3b** (Figure 2 and S18), **3c**, and **4b** the reactions were complete or near-complete in a few days and the temporal evolution of the A\*- spectra could be fitted to a second-order rate-law:

$$d[A^{\bullet-}]/dt = k_{H}[N-DMBI-H][A]$$
(8)

where  $k_{\rm H}$  is a rate constant, values for which are given in Table 2. For **3a**, **4a**, and **4c** the reactions were sufficiently sluggish that no reliable kinetic data could be obtained. For **5** no reaction was observed, consistent with previous work.<sup>29</sup>

Molecule **2** has a similar  $E^{0/\bullet-}$  to **3b**, but exhibits very different reactivity with **IaH**. Neutral **2** rapidly transforms into a green species with an absorption spectrum significantly different from that assigned to **2**\*- (Figure 3), although, as discussed further below, some **2**\*- is also obtained in variable quantities that depend on the reaction conditions. As described in the following section, this can be assigned to the hydride-reduced product, AH<sup>-</sup>; its formation can be fitted using eq. 9 (Figure S19).

$$d[AH^{-}]/dt = k_{H}[N-DMBI-H][A]$$



Rate constants for a series of similar reactions are often correlated with the driving force ( $-\Delta G^0$ ), as described by Marcus theory for the case of ET reactions, and, more generally, as inferred from extension of the Hammond postulate. Plots of  $k_{\rm H}$  vs. –  $\Delta G^0$  for electron, H<sup>\*</sup>, and H<sup>-</sup> transfers (Figure 4, S20) were examined for such correlations, while recognizing the possibility of different pathways for different acceptors. Firstly note that the DFT calculations indicate that, in solution, H- transfer is considerably more favorable in all cases than either electron or H\* transfer. Values of k<sub>H</sub> correlate poorly with electrochemical or DFT estimates of the driving force for ET,  $-\Delta G^{0}_{3}$ . In particular, **2** reacts much more rapidly than the cyano-rylene diimides (3b, 3c, 4b), despite similar reduction potentials and, therefore, similar values of –  $\Delta G^{0_3}$ ; similarly, **1** reacts more rapidly than **3b** and **4b**. The rate data correlate somewhat better with the DFT driving forces for H<sup>-</sup> and H<sup>•</sup> transfer,  $-\Delta G^{0_4}$  or  $-\Delta G^{0_5}$ , especially with solvent dielectric  $-\Delta G^{0}_{5}$  data, if one excludes **4c** and **5**, for both of which the most stable AH\* and AH\* isomers (Table S3) in the gas phase result from sterically hindered additions (see also caption of Figure S16) and thus may have particularly high activation barriers. In the case of 5, H° or H⁻ is added to an alkyne carbon, shielded by the Si<sup>i</sup>Pr<sub>3</sub> groups (solution minimization of these 5H<sup>\*</sup> and 5H<sup>-</sup> isomers was unsuccessful and so no  $-\Delta G^{0}_{4}$  or  $-\Delta G^{0}_{5}$  values for **5** are shown in Figure 4). The most stable gas-phase isomers of 4cH\* and 4cH\* result from addition to the Br-substituted C of 4c, which is hindered by the twist between the two naphthalene sub-units of the core. Minimization of these 4cH\* and 4cH\* isomers in solvent dielectric results in dissociation of Br\* or Br-; however, mass spectrometry of reaction mixtures did not show any dibrominated products, indicating that these substitution reaction do not occur to a significant extent under our experimental conditions, likely due to the activation barriers associated with the steric hindrance. The values of  $-\Delta G^{0}_{4}$  or  $-\Delta G^{0}_{5}$  for **4c** in Figure 4 are for the next most stable isomers, which do not dissociate, but which also involve a hindered addition.

Reactions involving photoexcited A or **IaH** are also in principle possible when reactions are carried out under visible or UV light (Figure S21). Indeed, ET from donors to photoexcited amide- and imide-based acceptors is reported, as exemplified by the reduction of **3** and **4** derivatives by simple alkyl amines, <sup>39</sup> and ET from UV-excited **IH** derivatives can be used in reductive organic transformations. <sup>40,41</sup> Here, laboratory light has no effect on the reactivity of **IaH** with acceptors such as **3a** and **3b** that exhibit little absorption in the visible region. UV light, however, significantly enhances the initial rate of formation of **3b**\*- (over ca. 20 min), presumably through excited-state ET, but further reaction under UV leads to decomposition of **3b**\*- and the formation of unknown products. No UV-induced formation of A\*- was seen for the reaction between **IaH** and **3a**; decomposition of **IaH**, accompanied by the evolution of structureless longer wavelength peaks was observed.

#### Reaction of Acceptors with N-DMBI-D

For the acceptors that react with **IaH** in the dark at a measureable rate, rate constants,  $k_D$ , were also determined using **IaD**;<sup>29</sup> in each case values of  $k_H/k_D$  (5.1–5.8; Table 2, Figures 2 and S19) indicated primary KIEs, indicative of hetero-or homolytic breaking of the bond to H/D in the RDS.

We also investigated the reaction products of **3b** with **IaH** and **IaD** using negative mode MALDI-TOF mass spectrometry (Figure S22). The different isotope patterns observed for the **3b**\*- ion indicate that ca. 20-30% of a monodeuterated anion is formed when **IaD** is used, providing direct evidence for the intermediacy of A(H/D)\* or A(H/D)\* species. The observed extent of deuteration is inconsistent with simple addition of D\* or D- to the CH position of the naphthalene ring, followed by loss of



(H/D)\* from that position. The KIE associated with A–H/D bond cleavage would be expected to favor H loss and thus lead to >>50% monodeuteration. On the other hand, addition to a different position, such as the cyano-substituted carbon of the naphthalene ring, followed by D\* loss would lead to no deuteration. The data are, therefore, consistent with addition occurring at multiple positions and/or with equilibration between different A(H/D)\* or A(H/D)\* isomers prior to [H/D] loss (see Figure S23).

#### Reaction Product of N-DMBI-H and 2CN-BDOPV

As noted above, compound  $\bf 2$  has significantly different reactivity with  $\bf laH$  to the other acceptors examined, yielding a green species distinct from the  $\bf 2^{\bullet -}$  that is obtained using the dimeric reductants. This species is stable for at least several days in benzene, toluene, and chlorobenzene in  $N_2$  atmosphere at room temperature and can even survive brief heating to  $100~^{\circ}$ C (Figure S30A-C). ESR spectra (Figure S15) show only weak signals attributable to traces of  $\bf 2^{\bullet -}$  (which are also observable in vis.-NIR experiments in small and variable quantities), while  $^{1}$ H and  $^{13}$ C NMR spectra are consistent with a diamagnetic species. These NMR signals can be accounted for by the presence of a ca. 1:1 mixture of  $\bf la^{\bullet}$  and a single isomer of  $\bf 2H^{-}$ . 1D and 2D  $^{1}$ H and  $^{13}$ C NMR spectra (see Figures S24-S29) indicate this to be the isomer shown in Figure 3B, which is also the most stable (by ca. 60 kJ mol $^{-1}$ ) according to DFT calculations.

Exposure of green **2H**<sup>-</sup> solutions to oxygen results in a slow transformation to gray-colored solutions with absorption spectra almost indistinguishable from those of **2**<sup>--</sup> obtained using dimeric dopants (Figure S30). The same spectra can be obtained by conducting the doping reaction in the presence of air, with **2H**<sup>-</sup> being observed as an intermediate. However, comparison of **Ia**<sup>+</sup> and **2H**<sup>-</sup> absorption features obtained when doping with 0.5 equiv. **(Ia)**<sub>2</sub> and 1 equiv. **IaH** in air indicate that only ca. 0.5 equiv. **2**<sup>--</sup> is obtained in the latter case (Figure S31). Moreover, **2**<sup>--</sup> is also formed under inert conditions in somewhat greater quantities when n-doping with < 1 equiv. **IaH**, i.e., when excess **2** is present (Figure S32).

#### **DISCUSSION**

#### Mechanism of N-DMBI-H Doping

Several studies have at least implied IH derivatives (or IH:A complexes) might initially lose free H\* to form I\*, which subsequently reacts through ET. 7,23,25 However, this reaction yields two high-energy products; DFT calculations suggest  $\Delta G^0$  for the conversion of IaH to Ia\* and 0.5H<sub>2</sub> is ca. +97 kJ mol<sup>-1</sup>, and the formation of H\* will of course be even more endergonic. Reactions have also been proposed for two high-EA pyrrolopyrrole-derived acceptors in which H\* is lost from a IaH:A charge-transfer (CT) complexes to form Ia+: A-- complexes, i.e., in which H- loss is coupled to formation of a tight ion pair.<sup>42</sup> The authors calculated these reactions to be enthalpically unfavorable ( $\Delta H^0$  = ca. +90 kJ mol<sup>-1</sup> for a quinoidal derivative with a very facile reduction potential of ca. -0.3 V vs. FeCp<sub>2</sub>+/0). The related reaction of two IaH:A complexes react to liberate H<sub>2</sub> would be less unfavorable. Although reaction via CT complexes may be viable for some acceptors under certain conditions, these pathways are unlikely to be relevant in the present context since our UV-vis.-NIR spectra show no evidence for CT complex formation between IaH and A at short reaction times, or (for acceptors that do react to a significant extent) between la+ and A<sup>•-</sup> at long reaction times. Moreover, generation of H<sup>•</sup> or H<sub>2</sub> from **IaH** or from CT complexes would account for neither the observation of deuterium incorporation from IaD into 3b nor the direct observation of 2H-. Accordingly, we do not consider



these reactions further, but as the first step of the reaction of **IaH** with any given A in the dark we consider only electron,  $H^{\bullet}$ , and  $H^{-}$  transfer (eq. 3-5, respectively).

ET reactions involving **IH** derivatives include the reductive dehalogenation of  $\alpha$ -haloketones by **IbH** through radical-chain reactions initiated by endergonic ET, <sup>43</sup> while **IbH\*** has been observed by ESR when generated with Fe(bpy)<sub>3</sub><sup>3+</sup> at low temperature. <sup>9</sup> H\* transfer is involved in chain reactions between **IH** derivatives and substrates such as  $\alpha$ -haloketones; <sup>43</sup> in these a high-energy radical reacts with **IH** to form high-energy **I\*** and a closed-shell molecule, but in the reaction of eq. 4, two high-energy radicals are formed and the reaction is calculated to be significantly endergonic in both gas phase and in solvent dielectric. Finally, H<sup>-</sup> transfer takes place in multiple reactions of **IH** derivatives, <sup>9,44-46</sup> including the reduction of **1**,<sup>29</sup> and the reactions of eq. 5 are calculated to be significantly more endergonic in solvent dielectric than those of eq. 4.

ET (eq. 3) from IaH, at least to some of the stronger electron acceptors considered here, does not appear prohibitively endergonic. Thus, although IaH is a weak oneelectron donor relative to the dimeric dopants,  $\Delta G^{0}_{3}$  for ET from **IaH** to **3b** (40 kJ mol<sup>-1</sup> according to electrochemical data) is only a little larger than that for ET from (II)<sub>2</sub> to 5 (+34 kJ mol<sup>-1</sup>)<sup>34</sup> and smaller than that for the reaction of (Ic)<sub>2</sub> with 5 (+78 kJ  $\text{mol}^{-1}$ ), 35 both of which proceed with rate constants,  $k \sim 10 \text{ M}^{-1} \text{ min}^{-1}$ . However, an ET RDS for the reaction of laH with the cyano-rylene diimides 3b, 3c, and 4b is ruled out by the large primary KIEs. An ET step, followed by a RDS in which H<sup>o</sup> is lost from IaH\*\* (to, for example, solvent) would be consistent with the KIE, but is inconsistent with the observed incorporation of deuterium into 3b. Thus, the first step for the reaction of IaH with 3b and other rylene diimides is either H\* or Htransfer; although the former cannot be ruled out based on the purely experimental data presented here, we consider H- transfer the most likely reaction. DFT calculations that include the solvent dielectric suggest that for each acceptor Htransfer is less endergonic than either electron or H\* transfer (Table 1); indeed, hydride transfer is calculated to be endergonic for the cyano-rylene diimides. Furthermore, the free energies of activation,  $\Delta G^{\dagger}$ , obtained from the observed values of  $k_H$  for **3b**, **3c**, and **4b** (74, 81, and 80 kJ mol<sup>-1</sup>, respectively) and the Eyring equation are much smaller than the corresponding free energies of reaction for H\* transfer,  $\Delta G^{0}_{4}$  (Table 1) from solvent-dielectric DFT, thus implying the experimental data are more likely to represent hydride transfers in each case. The H<sup>-</sup> transfers may well be the RDS, although in principle the observed KIEs could also be accounted for if a subsequent H\* transfer from AH- to some other species was the RDS. Evidently, the initially formed AH<sup>-</sup> or AH<sup>•</sup> is rapidly converted to A<sup>•-</sup>, which, besides N-DMBI<sup>+</sup>, is the only product detected and overall is formed stoichiometrically from A. The mechanism by which [H] is lost from the rylene diimide AH\* or AH\* species and the final fate of that hydrogen are unclear. In the case of 1, we have previously suggested that an ET between AH<sup>-</sup> and A,

$$AH^{-} + A = AH^{\bullet} + A^{\bullet -}$$
 (10)

leads to the formation of A\*-, with AH\* reacting further to ultimately form multiply hydrogenated PCBM as an observable side product. In the case of the cyano-rylene diimides (**3b**, **3c**, and **4b**), the unlikelihood of forming highly hydrogenated products, the stoichiometric formation of A\*-, and the lack of any observable side products suggest a different fate for [H]. AH\*, either formed directly in a first step (eq. 4) or, more likely, by the reaction of A and AH-(eq. 10, which, as shown in Figure 5 and Table S3), may react with another AH\* molecule,

$$2AH^{\bullet} \rightarrow 2A + H_2 \tag{11}$$

with the resulting A subsequently undergoing another hydride transfer with **IaH**. Alternatively, AH\* may react with another dopant molecule,

$$AH^{\bullet} + DH \rightarrow A + H_2 + D^{\bullet}$$
 (12)

with subsequent highly exergonic ET from  $\mathbf{la}^{\bullet}$  to A. These two possible pathways for  $H_2$  formation are shown in Figure 5A, along with DFT-calculated free energies for these two possibilities in Figure 5C for the case of  $\mathbf{3b}$ , suggesting that reaction according to eq. 11 (exergonic) is more likely than via eq. 12 (highly endergonic).

The behavior of the amide/ester compound  ${\bf 2}$  is fundamentally different from that of the rylene diimides ( ${\bf 3}$ ,  ${\bf 4}$ ) or PCBM ( ${\bf 1}$ ) in that the hydride-reduced species, AH-, is directly observable and can (depending on the exact reaction conditions) be formed quite cleanly under inert atmosphere, providing experimental as well as computational evidence, that the net H- transfer (eq. 5) is thermodynamically favorable; indeed DFT calculations indicate that H- reduction of  ${\bf 2}$  is more thermodynamically favorable than for any of the other acceptors considered here. The KIE indicates that this proceeds either by H- transfer (i.e. concerted electron and H\* transfer), or by sequential electron/H\* or H\*/electron transfers, with H\* transfer the RDS, although, as with the cyano-rylene diimides, the DFT calculations in solvent suggest H- transfer would be more likely (again the calculated value of  $\Delta G^0$  for H\* transfer is larger than than that of  $\Delta G^{\ddagger}$  (58 kJ mol-1) inferred from the observed rate constant).

The failure of the principal initial reduction product of 2 (in contrast to those of 1, 3, and 4) to spontaneously convert to A\*- partly arises from the stability of 2H-, and indicates that the initial formation of 2H<sup>-</sup> is very fast compared to any subsequent reactions, such as the reaction of eq. 10 followed by those of eq. 11 or eq. 13. Indeed, the formation of 2H<sup>-</sup> is fast relative to the reaction of the other acceptors, whereas the reaction represented by eq. 10, as shown in Table S3 and in Figure 5B, is calculated to be significantly more endergonic, and, therefore, likely slower, for 2 than for the cyano-rylene diimides, **3b**, **3c**, and **4b**. Under such conditions, the H<sup>-</sup> transfer reaction may be complete before significant subsequent reaction can take place; when ≥1 eq of dopant is used no neutral 2 will be available to enable formation of 2H\* through eq. 10. Moreover, the low yields of 2\*- obtained (ca. 15%) conversion of 2H<sup>-</sup> to 2\*- when using 0.5 eq. IaH, see Figure S31) indicate that, if 2H\* is indeed formed via eq. 10, it is not irreversibly lost through eq. 11 either. It is possible that this second step is rendered irreversible by reaction of 2H° with a trace impurity (which suggests that even lower proportions of 2°- might be formed at device-relevant concentrations, as indeed is the case at NMR concentrations). An intriguing feature of 2 reduction by IaH is that 2° is formed in ca. 50% yield when the reduction is carried out in air (Figure S31), or when 2H- is exposed to air (Figure S30D). The details of this reaction are unknown, but in Figure S34 we have suggested a possible scheme.

To summarize, reaction of **IaH** with acceptors (A) that are in principle reducible by **Ia** can result in at least four possible outcomes:

- (a) No measurable reaction (A = 5) or very slow reaction (A = 3a, 4a, 4c);
- (b) Initial H<sup>-</sup> transfer; AH<sup>-</sup> not directly observable, due to a fast second step forming A\*-; and AH<sub>x</sub> side products detected (A =  $\mathbf{1}$ );



- (c) Initial H<sup>-</sup> or H<sup>•</sup> transfer (likely the former); AH<sup>-</sup>/AH<sup>•</sup> not directly observable, due to a fast second step forming 1 eq. A<sup>•-</sup>; and AH<sub>x</sub> side products not detected with final fate of H unknown, but perhaps lost as H<sub>2</sub> (A = **3b**, **3c**, **4b**);
- (d) Initial net H<sup>-</sup> transfer; AH<sup>-</sup> observable and stable under certain conditions; final fate of H unknown under conditions where AH<sup>-</sup> is converted to 0.5 equiv. A\*- and unknown side products (A = **2**).

#### **Implications for Selection of Dopants and Doping Conditions**

While  $E^{0'^{\bullet-}}(A)$  is a useful predictor of the feasibility of n-doping A using a simple one-electron reductant, our results emphasize that it does not correlate well with the rates of reaction with IaH, or with which of the four outcomes mentioned above is observed. The stability of AH<sup>-</sup> in the case of **2** highlights the possibility that IaH and similar dopants, even when reactive with A, do not necessarily form A<sup>•-</sup>, as desired when n-doping. Furthermore, **2H**<sup>-</sup> absorbs at longer wavelengths than neutral **2** and, without comparison to the reduction product obtained using a one-electron reductant, or the use of NMR and/or ESR spectroscopy, could potentially be misidentified as **2**<sup>•-</sup>. The effect of oxygen in increasing the yield of **2**<sup>•-</sup> is also unexpected; typically n-doped films are prepared and handled under inert atmosphere due to the sensitivity of many A<sup>•-</sup> species to oxygen and/or water. Indeed **2**<sup>•-</sup> is still somewhat air-sensitive and, in any case, its formation when using IaH must be accompanied by formation of another unknown **2**-derived material.

In addition, where  $A^{\bullet}$  is formed, [H]-containing side-products (the identity of which is unknown, but which could change depending on the acceptor in question, solvent and other processing conditions) are inevitably formed when using **IaH**. If the side product is H<sub>2</sub> it will be readily lost; however, other side products may be incorporated into films when doping and may in some cases adversely affect the electronic properties of the doped films.

Thus, although **IaH** can, in many cases, act as a useful n-dopant affording desirable electrical properties, there are significant drawbacks to its general use as an n-dopant, even for organic semiconductors with relatively facile reductions ( $E(A^{0^{\bullet-}}) \ge ca. -1 \text{ V}$  vs.  $FeCp_2^{+/0}$ ). Many of these drawbacks can be avoided by using simple one-electron reductants, which are generally, however, highly sensitive to ambient conditions, or by using dimeric dopants,  $D_2$ , which exhibit intermediate sensitivity. The outcome of the reaction of acceptors with both these classes of dopants – which, if they react, cleanly afford  $A^{\bullet-}$  and  $D^+$  as the only products – can, for a given dopant, be readily be predicted based on  $E(A^{0^{\bullet-}})$  alone. Indeed, (Ia)<sub>2</sub> and (II)<sub>2</sub> reduce all A considered here, including 5, to give  $A^{\bullet-}$  as the only detectable Aderived product (Figure S14), the reactions all occurring much more rapidly than those using IaH.

On the other hand, it is worth noting that in some cases slow reaction rates can be advantageous; for example, if dopant and semiconductor are to be mixed in solution prior to film casting and the resulting D+A+ salt is poorly soluble, precipitation may be observed prior to casting or highly heterogeneous films may be obtained (as seen, for example, in some p-doping experiments<sup>47</sup>). A possible solution to this problem is to use a dopant that reacts slowly prior to spin coating (while bearing in mind that second-order reactions will proceed much more rapidly at typical casting concentrations than at those used in the present spectroscopic work), but that could subsequently be driven to react more completely by the relatively high concentrations in the film or in the final stages of film deposition, or



by a subsequent heating. Indeed, although P(NDIOD-T2) (Figure 1) and related polymers have frequently been doped using **IH** derivatives, <sup>13,16,25,48</sup> in many cases, including solution vis.-NIR studies, negligible solution reactivity is evident (consistent with our findings for **3a**), while a high-temperature (>100 °C) annealing step is generally, although not universally, employed prior to measurement of conductivity. Dopant / semiconductor combinations that require subsequent annealing may also enable film deposition to be carried out in air, even when A<sup>--</sup> is significantly air sensitive. Nevertheless, it should be reiterated that whether rapid or slow kinetics are desired, they are not easily predicted for the reaction of a new acceptor and **IaH**.

For n-doping of films, another consideration is the size and shape of the dopant ions. Bulkier ions are likely to be less prone to diffusion and may also be shallower electrostatic traps for carriers. On the other hand, in some cases, higher conductivity values have been obtained using smaller or more planar dopants: IaH affords higher conductivity than (II)<sub>2</sub> in FBDPPV, and this difference has been attributed to greater disruption of the host structure by the bulky 3D II<sup>+</sup> ions than by the more planar Ia<sup>+</sup>. The recent developed (Ia)<sub>2</sub> exhibits similar chemistry to (II)<sub>2</sub>, but forms the same ion as IaH, a combination of properties recently exploited in efficient doping of FBDPPV. Despite synthesis that is more hazardous than that of IaH, requiring the use of Na:Hg under inert atmosphere, and its moderate air sensitivity, (Ia)<sub>2</sub> will likely be a preferable dopant to IaH in many cases, due to its generally greater dopant strength and its cleaner and more predictable reactivity.

#### **Conclusions**

The reaction rates between N-DMBI-H, IaH, and a range of acceptors, A, with reduction potentials in the range -0.54 to -1.10 V vary by many orders of magnitude and these rate constants do not correlate well with E(A<sup>0/•-</sup>) or the DFTcalculated hydride- or hydrogen-accepting strength of the acceptors. In the case of 2, a H<sup>-</sup>-reduced species is formed rapidly as the major product; this intermediate is remarkable stable and is only converted to A\*- in the presence of excess A or molecular oxygen. For the other acceptors examined, AH- or other hydrogenreduced species are not directly observed. However, kinetic isotope effects (where measured) are consistent with a rate-determining hydride- or hydrogen-atomtransfer step, followed by rapid conversion of AH- or AH• to A•-. DFT calculations suggest that an initial hydride transfer is considerably more favorable than a hydrogen-atom transfer when the presence of solvent is taken into account, and that AH<sup>-</sup> and A may react further to form AH<sup>•</sup> and A<sup>•-</sup>, with AH<sup>•</sup> undergoing H<sub>2</sub> loss. These results emphasize the difficulties in predicting the suitability of hydride-donor reductants such as IaH with a given acceptor. In contrast, all the acceptors examined here are rapidly reduced by the dimeric analogue of IaH, (Ia)2.17

#### **EXPERIMENTAL PROCEDURES**

#### **Lead Author**

Further information and requests for resources and reagents should be directed to and will be fulfilled by the Lead Contact, Stephen Barlow (stephen.barlow@chemistry.gatech.edu).

#### **Materials Availability**

2CN-BDOPV (2) generated as part of this study will be made available on request, but we may require a payment and/or a completed Materials Transfer Agreement if there is potential for commercial application.





#### **Data and Code Availability**

The published article and the Supplemental Information include all data generated or analyzed during this study.

#### Synthesis, Characterization, Kinetic Measurements, and DFT Calculations

The procedures are described in the Supplemental Information.

#### SUPPLEMENTAL INFORMATION

Document S1. Figures S1–S34, Table S1-S4, Supplemental Experimental Procedures, and References for Supplemental Information.

#### **ACKNOWLEDGMENTS**

This work was supported by: the National Science Foundation (through DMR-1807797 and DMR-1729737); the United States-India Educational Foundation and Institute of International Education (through a Fulbright-Nehru Postdoctoral Fellowship to S. J., Grant No. 2266/FNPDR/2017); the National Natural Science Foundation of China (through 21790360, 21722201, and 21420102005); the Office of Naval Research Young Investigator Program (N00014-18-1-2448); and the University of Kentucky Information Technology Department and Center for Computational Sciences (CCS) (for provision of supercomputing resources on the Lipscomb High Performance Computing Cluster). We thank Khaled Al Kurdi for providing 3c, Ye-Xin Wang for assistance with ESR measurements, and Yadong Zhang for providing the oxidant used for Figure S13C.

#### **AUTHOR CONTRIBUTIONS**

Conceptualization, J. P., S. B., and S. R. M.; Investigation, S. J., H.-I. U., Y.-F. D., and C. R.; Resources, S. K. M., Writing – Original Draft, S. J., H.-I. U., and S. B.; Writing – Review and Editing, all authors; Funding Acquisition – C. R., J. P., S. R. M., and S. B.; Supervision, J. P., S. B., and S. R. M.

#### **DECLARATION OF INTERESTS**

S. K. M., S. B., and S. R. M. are inventors on a patent (U.S. Patent 8,912,535) relating to the use of  $II_2$  as an n-dopant.

#### **REFERENCES**

- Walzer, K., Maenning, B., Pfeiffer, M., and Leo, K. (2007). Highly efficient organic devices based on electrically doped transport materials. Chem. Rev. 107, 1233-1271.
- Lüssem, B., Tietze, M.L., Kleemann, H., Hoßbach, C., Bartha, J.W., Zakhidov, A., and Leo, K. (2013).
   Doped organic transistors operating in the inversion and depletion regime. Nat. Commun. 4, 2775.
- Russ, B., Glaudell, A., Urban, J.J., Chabinyc, M.L., and Segalman, R.A. (2016). Organic thermoelectric materials for energy harvesting and temperature control. Nat. Rev. Mater. 1, 16050.
- Wang, Z.-K., and Liao, L.-S. (2018). Doped charge-transporting layers in planar perovskite solar cells. Adv. Opt. Mater. 6, 1800276.
- 5. Chan, C.K., Kahn, A., Zhang, Q., Barlow, S., and Marder, S.R. (2007). Incorporation of cobaltocene as an n-dopant in organic molecular films. J. Appl. Phys. 102, 014906.
- Li, F., Werner, A., Pfeiffer, M., Leo, K., and Liu, X. (2004). Leuco crystal violet as a dopant for ndoping of organic thin films of fullerene C<sub>60</sub>. J. Phys. Chem. B 108, 17076-17082.
- Wei, P., Oh, J.H., Dong, G., and Bao, Z. (2010). Use of a 1*H*-benzoimidazole derivative as an *n*-type dopant and to enable air-stable solution-processed *n*-channel organic thin-film transistors. J. Am. Chem. Soc. 132, 8852-8853.
- 8. Reddy, A.P.R., Veeranagaiah, V., and Ratnam, C.V. (1985). Synthesis and autoxidation of 1,3-dialkyl-2-arylbenzimidazolines. Ind. J. Chem. *B24*, 367-371.



- 9. Zhu, X.-Q., Zhang, M.-T., Yu, A., Wang, C.-H., and Cheng, J.-P. (2008). Hydride, hydrogen atom, proton, and electron transfer driving forces of various five-membered heterocyclic organic hydrides and their reaction intermediates in acetonitrile. J. Am. Chem. Soc. *130*, 2501-2516.
- Rosas-Hernández, A., Steinlechner, C., Junge, H., and Beller, M. (2017). Earth-abundant photocatalytic systems for the visible-light-driven reduction of CO<sub>2</sub> to CO. Green Chem. 19, 2356-2360.
- Lu, M., Nicolai, H.T., Wetzelaer, G.-J.A.H., and Blom, P.W.M. (2011). n-Type doping of poly(p-phenylene vinylene) with air-stable dopants. Appl. Phys. Lett. 99, 173302.
- Naab, B.D., Himmelberger, S., Diao, Y., Vandewal, K., Wei, P., Lussem, B., Salleo, A., and Bao, Z. (2013). High mobility n-type transistors based on solution-sheared doped 6,13-bis(triisopropylsilylethynyl)pentacene thin films. Adv. Mater. 25, 4663-4667.
- Schlitz, R.A., Brunetti, F.G., Glaudell, A.M., Miller, P.L., Brady, M.A., Takacs, C.J., Hawker, C.J., and Chabinyc, M.L. (2014). Solubility-limited extrinsic n-type doping of a high electron mobility polymer for thermoelectric applications. Adv. Mater. 26, 2825-2830.
- Shi, K., Zhang, F., Di, C.-A., Yan, T.-W., Zou, Y., Zhou, X., Zhu, D., Wang, J.-Y., and Pei, J. (2015).
   Toward high performance n-type thermoelectric materials by rational modification of BDPPV backbones. J. Am. Chem. Soc. 137, 6979-6982.
- Guo, Y., Sato, W., Inoue, K., Zhang, W., Yu, G., and Nakamura, E. (2016). n-Type doping for efficient polymeric electron-transporting layers in perovskite solar cells. J. Mater. Chem. A 4, 18852-18856.
- Saglio, B., Mura, M., Massetti, M., Scuratti, F., Beretta, D., Jiao, X., McNeill, C.R., Sommer, M., Famulari, A., Lanzani, G., et al. (2018). N-Alkyl substituted 1H-benzimidazoles as improved n-type dopants for a naphthalenediimide based copolymer. J. Mater. Chem. A 6, 15294-15302.
- Un, H.-I., Gregory, S.A., Mohapatra, S.K., Xiong, M., Longhi, E., Lu, Y., Rigin, S., Jhulki, S., Yang, C.-Y., Timofeeva, T.V., et al. (2019). Understanding the effects of molecular dopant on n-type organic thermoelectric properties. Adv. Energy Mater. 9, 1900817.
- Lu, Y., Yu, Z.-D., Zhang, R.-Z., Yao, Z.-F., You, H.-Y., Jiang, L., Un, H.-I., Dong, B.-W., Xiong, M., Wang, J.-Y., et al. (2019). Rigid coplanar polymers for stable n-type polymer thermoelectrics. Angew. Chem. Int. Ed. 58, 11390-11394.
- 19. Yan, X., Xiong, M., Li, J.-T., Zhang, S., Ahmad, Z., Lu, Y., Wang, Z.-Y., Yao, Z.-F., Wang, J.-Y., Gu, X., et al. (2019). Pyrazine-flanked diketopyrrolopyrrole (DPP): A new polymer building block for high-performance n-type organic thermoelectrics. J. Am. Chem. Soc. 141, 20215-20221.
- Wei, P., Liu, N., Lee, H.R., Adijanto, E., Ci, L., Naab, B.D., Zhong, J.Q., Park, J., Chen, W., Cui, Y., et al. (2013). Tuning the Dirac point in CVD-grown graphene through solution processed n-type doping with 2-(2-methoxyphenyl)-1,3-dimethyl-2,3-dihydro-1*H*-benzoimidazole. Nano Lett. 13, 1890-1897.
- Heo, J.S., Kim, T., Ban, S.-G., Kim, D., Lee, J.H., Jur, J.S., Kim, M.-G., Kim, Y.-H., Hong, Y., and Park, S.K. (2017). Thread-like CMOS logic circuits enabled by reel-processed single-walled carbon nanotube transistors via selective doping. Adv. Mater. 29, 1701822.
- Tarasov, A., Zhang, S., Tsai, M.-Y., Campbell, P.M., Graham, S., Barlow, S., Marder, S.R., and Vogel, E.M. (2015). Controlled doping of large-area trilayer MoS<sub>2</sub> with molecular reductants and oxidants. Adv. Mater. 27, 1175-1181.
- 23. Bin, Z., Li, J., Wang, L., and Duan, L. (2016). Efficient n-type dopants with extremely low doping ratios for high performance inverted perovskite solar cells. Energy Environ. Sci. 9, 3424-3428.
- Zhang, S., Moudgil, K., Jucov, E., Risko, C., Timofeeva, T.V., Marder, S.R., and Barlow, S. (2019).
   Organometallic hydride-transfer agents as reductants for organic semiconductor molecules. Inorg. Chim. Acta 489, 67-77.
- 25. Riera-Galindo, S., Biroli, A.O., Forni, A., Puttisong, Y., Tessore, F., Pizzotti, M., Pavlopoulou, E., Solano, E., Wang, S., Wang, G., et al. (2019). Impact of singly occupied molecular orbital energy on the n-doping efficiency of benzimidazole derivatives. ACS Appl. Mater. Interf. 11, 37981-37990.
- Uebe, M., Yoshihashi, Y., Noda, K., Matsubaraa, M., and Ito, A. (2018). A dendritic oligoarylaminesubstituted benzimidazole derivative as a useful n-type dopant. J. Mater. Chem. C 6, 6429-6439.
- Qiu, L., Liu, J., Alessandri, R., Qiu, X., Koopmans, M., Havenith, R.W.A., Marrink, S.J., Chiechi, R.C., Anton Koster, L.J., and Hummelen, J.C. (2017). Enhancing doping efficiency by improving host-dopant miscibility for fullerene-based n-type thermoelectrics. J. Mater. Chem. A 5, 21234-21241.
- 28. Reiser, P., Benneckendorf, F.S., Barf, M.-M., Müller, L., Bäuerle, R., Hillebrandt, S., Beck, S., Lovrincic, R., Mankel, E., Freudenberg, J., et al. (2019). n-Type doping of organic semiconductors: Immobilization via covalent anchoring. Chem. Mater. 31, 4213-4221.
- Naab, B.D., Guo, S., Olthof, S., Evans, E.G.B., Wei, P., Millhauser, G.L., Kahn, A., Barlow, S., Marder, S.R., and Bao, Z. (2013). Mechanistic study on the solution-phase n-doping of 1,3dimethyl-2-aryl-2,3-dihydro-1*H*-benzoimidazole derivatives. J. Am. Chem. Soc. *135*, 15018–15025.
- 30. Guo, X., Facchetti, A., and Marks, T.J. (2014). Imide- and amide-functionalized polymer semiconductors. Chem. Rev. 114, 8943-9021.
- 31. Lei, T., Xia, X., Wang, J.-Y., Liu, C.-J., and Pei, J. (2014). "Conformation locked" strong electrondeficient poly(p-phenylene vinylene) derivatives for ambient-stable n-type field-effect transistors:



- Synthesis, properties, and effects of fluorine substitution position. J. Am. Chem. Soc. 136, 2135-2141.
- Anthony, J.E., Brooks, J.S., Eaton, D.L., and Parkin, S.R. (2001). Functionalized pentacene: Improved electronic properties from control of solid-state order. J. Am. Chem. Soc. 123, 9482-9483.
- 33. Sheraw, C.D., Jackson, T.N., Eaton, D.L., and Anthony, J.E. (2003). Functionalized pentacene active layer organicthin-film transistors. Adv. Mater. 15, 2009-2011.
- Guo, S., Mohapatra, S.K., Romanov, A., Timofeeva, T.V., Hardcastle, K.I., Yesudas, K., Risko, C., Brédas, J.-L., Marder, S.R., and Barlow, S. (2012). N-doping of organic electronic materials using air-stable organometallics: A mechanistic study of reduction by dimeric sandwich compounds. Chem. Eur. J. 18, 14760-14772.
- Zhang, S., Naab, B.D., Jucov, E.V., Parkin, S., Evans, E.G.B., Millhauser, G.L., Timofeeva, T.V., Risko, C., Brédas, J.-L., Bao, Z., et al. (2015). N-dopants based on dimers of benzimidazoline radicals: Structures and mechanism of redox reactions. Chem. Eur. J. 21, 10878-10885.
- Gusev, O.V., Ievlev, M.A., Peterleitner, M.G., Peregudova, S.M., Denisovich, L.I., Petrovskii, P.V., and Ustynyuk, N.A. (1997). Reactions of ruthenium arenecyclopentadienyl complexes. Reactions induced by electron transfer. J. Organomet. Chem. 534, 57-66.
- Mohapatra, S.K., Fonari, A., Risko, C., Yesudas, K., Moudgil, K., Delcamp, J.H., Timofeeva, T.V., Brédas, J.-L., Marder, S.R., and Barlow, S. (2014). Dimers of nineteen-electron sandwich compounds: Crystal and electronic structures, and comparison of reducing strengths. Chem. Eur. J. 20, 15385–15394.
- Gosztola, D., Niemczyk, M.P., Svec, W., Lukas, A.S., and Wasielewski, M.R. (2000). Excited doublet states of electrochemically generated aromatic imide and diimide radical anions. J. Phys. Chem. A 104. 6545-6551.
- Tauber, M.J., Kelley, R.F., Giaimo, J.M., Rybtchinski, B., and Wasielewski, M.R. (2006). Electron hopping in π-stacked covalent and self-assembled perylene diimides observed by endor spectroscopy. J. Am. Chem. Soc. 128, 1782-1783.
- Hasegawa, E., Kato, T., Kitazume, T., Yanagi, K., Hasegawa, K., and Horaguchi, T. (1996). Photoinduced electron transfer reactions of a,b-epoxy ketones with 2-phenyl-N,N-dimethylbenzimidazoline (PDMBI): Significant water effect on the reaction pathway. Tetrahedron Lett. 37, 7079-7082.
- Igarashi, T., Tayama, E., Iwamoto, H., and Hasegawa, E. (2013). Carbon-carbon bond formation via benzoyl umpolung attained by photoinduced electron-transfer with benzimidazolines. Tetrahedron Lett. 54, 6874-6877.
- 42. Zeng, Y., Zheng, W., Guo, Y., Han, G., and Yi, Y. (2020). Doping mechanisms of N-DMBI-H for organic thermoelectrics: Hydrogen removal vs hydride transfer. J. Mater. Chem. A, 8, 8323-8328.
- Tanner, D.D., and Chen, J.J. (1989). On the mechanism of the reduction of α-halo ketones by 1,3dimethyl-2-phenylbenzimidazoline. Reduction by a set-hydrogen atom abstraction chain mechanism. J. Org. Chem. 54, 3842-3846.
- Chikashita, H., Ide, H., and Itoh, K. (1986). 1,3-dimethyl-2-phenylbenzimidazoline as a novel and
  efficient reagent for mild reductive dehalogenation of -halo carbonyl compounds and acid
  chlorides. J. Org. Chem. 51, 5400-5405.
- 45. Shen, G.-B., Xia, K., Li, X.-T., Li, J.-L., Fu, Y.-H., Yuan, L., and Zhu, X.-Q. (2016). Prediction of kinetic isotope effects for various hydride transfer reactions using a new kinetic model. J. Phys. Chem. A 120, 1779-1799.
- 46. Ma, L., Sakhaee, N., Jafari, S., Wilhelm, S., Rahmani, P., and Lu, Y. (2019). Imbalanced transition states from  $\alpha$ -H/D and remote  $\beta$ -type N-CH/D secondary kinetic isotope effects on the NADH/NAD $^+$  analogues in their hydride tunneling reactions in solution. J. Org. Chem. 84, 5431–5439.
- Dai, A., Zhou, Y., Shu, A.L., Mohapatra, S.K., Wang, H., Fuentes-Hernandez, C., Zhang, Y., Barlow, S., Loo, Y.-L., Marder, S.R., et al. (2014). Enhanced charge-carrier injection and collection via lamination of doped polymer layers p-doped with a solution-processible molybdenum complex. Adv. Funct. Mater. 24, 2197–2204.
- Kiefer, D., Giovannitti, A., Sun, H., Biskup, T., Hofmann, A., Koopmans, M., Cendra, C., Weber, S., Koster, L.J.A., Olsson, E., et al. (2018). Enhanced n-doping efficiency of a naphthalenediimidebased copolymer through polar side chains for organic thermoelectrics. ACS Energy Lett. 3, 278-285.

#### FIGURE TITLES ETC.

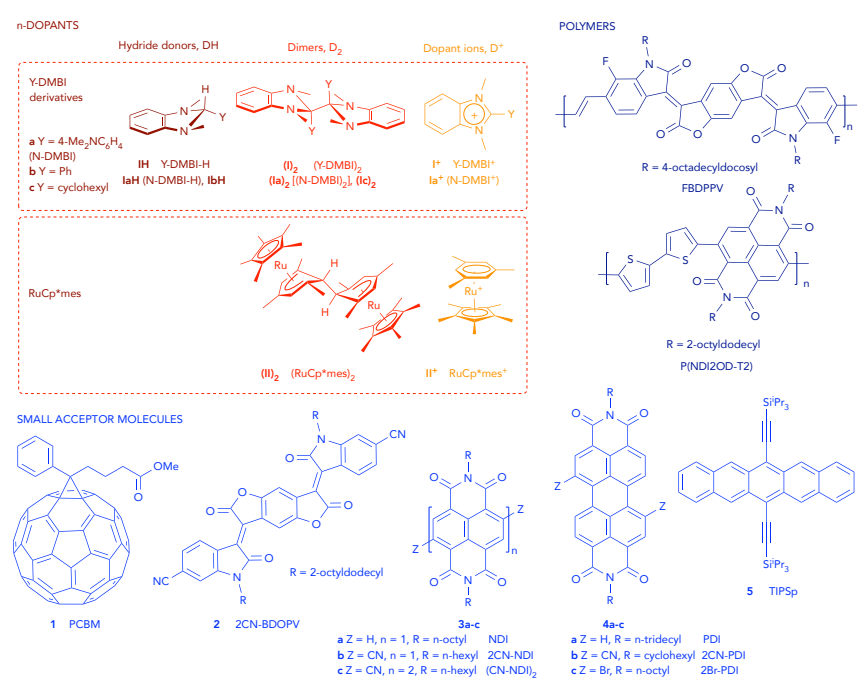


Figure 1. Chemical Structures of Dopants, Dopant Ions, Acceptor Molecules, and Polymers Referred to in this Work

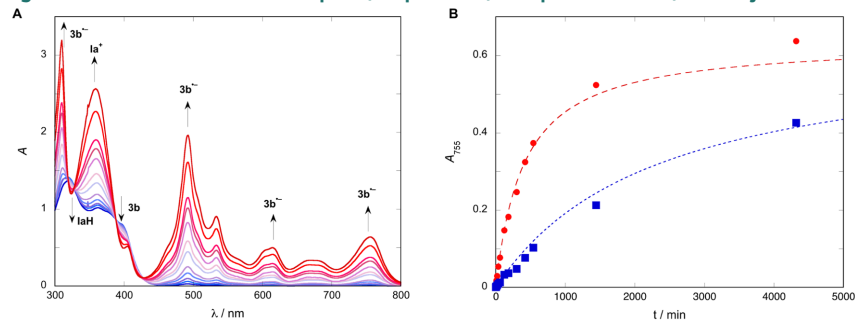


Figure 2. Solution Reactivity of N-DMBI-H and 2CN-NDI

(A) UV-vis.-NIR spectra in chlorobenzene showing conversion of 2CN-NDI, **3b**, to **3b**<sup>--</sup> subsequent to treatment with 1 equiv. N-DMBI-H, **IaH**.

(B) Temporal evolution of absorbance at 755 nm (one of the absorption maxima for **3b**<sup>--</sup>) for the reaction of **3b** and **IaH** (red circles) and **IaD** (blue squares), with fits to eq. 8 shown as dotted lines.

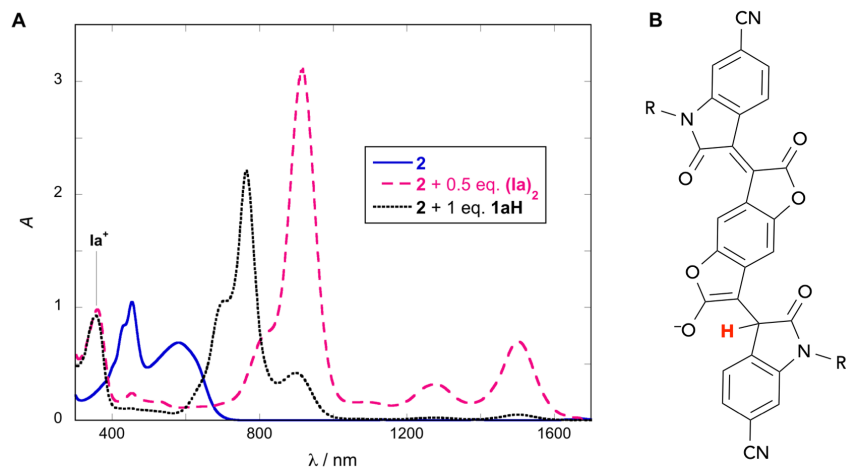


Figure 3. Absorption Spectra of 2CN-BDOPV Derivatives



(A) UV-vis.-NIR spectra in dry and deoxygenated chlorobenzene of 2CN-BDOPV, **2**, and of the products of its reaction with 0.5 equiv. (N-DMBl)<sub>2</sub>, (Ia)<sub>2</sub>, and 1 equiv. (N-DMBI-H), IaH, which are assigned to **2**<sup>--</sup>, and to primarily **2H**<sup>-</sup> (with a small quantity of **2**<sup>--</sup>), respectively.

(B) Chemical structure of the isomer of **2H**<sup>-</sup> that is the principal product of doping with **IaH** under inert atmosphere.

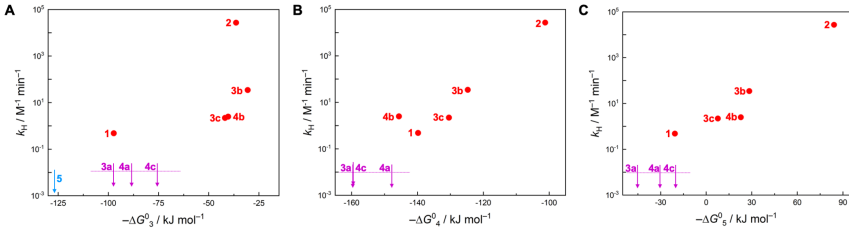


Figure 4. Dependence of Reaction Rates on Driving Forces

Semi-logarithmic plots of rate constants for the formation of  $A^-$  or, in the case of **2**,  $AH^-$  from A and N-DMBI-H, IaH, in chlorobenzene against the driving forces  $(-\Delta G^0)$  for (A) electron, (B)  $H^+$ , and (C)  $H^-$  transfer obtained from solution-phase M06/6-31G(d,p)/LANL2DZ DFT calculations. Values of  $-\Delta G^0$ <sub>4</sub> and  $-\Delta G^0$ <sub>5</sub> are for the more stable isomers of  $AH^+$  and  $AH^-$  respectively, except for **4c**, where  $Br^+$  or  $Br^-$  dissociation is found in solution; no values of these quantities were obtained for **5**, since the geometries of the most stable gas-phase isomers did not successfully converge when the solvent dielectric was included.

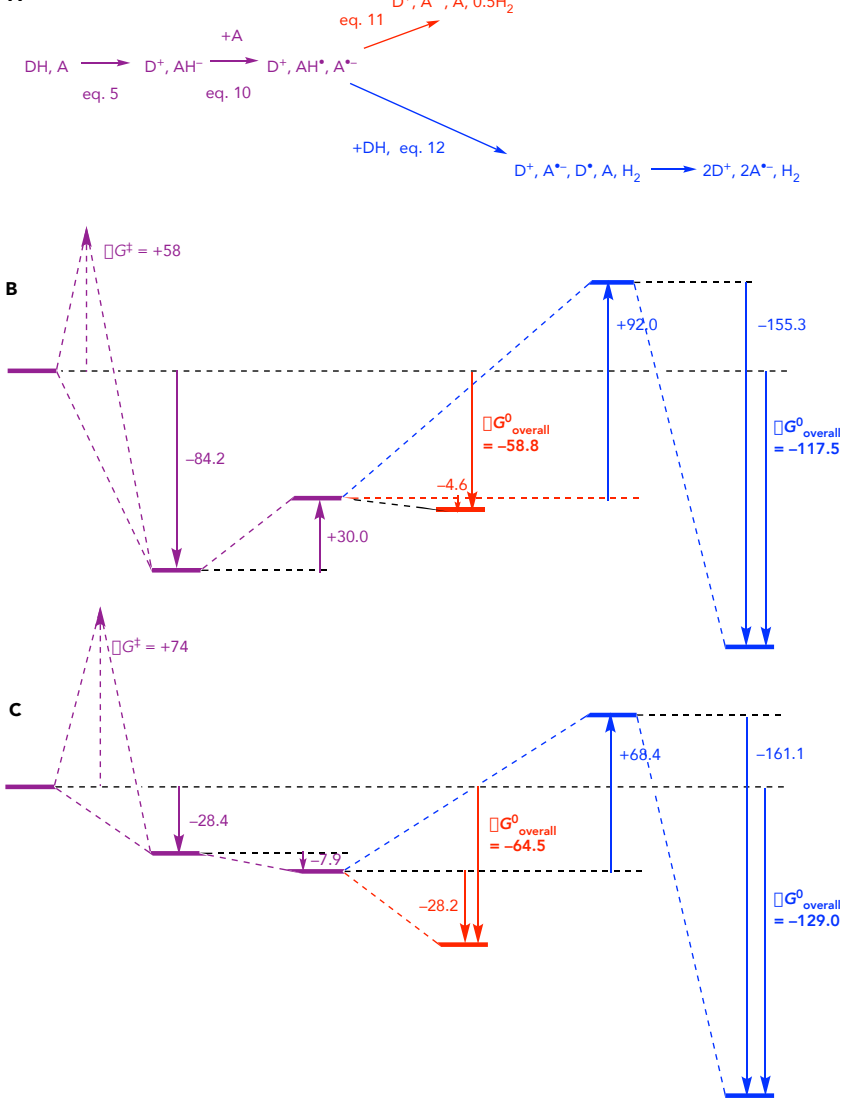


Figure 5. Free-Energies for Alternative Reaction Pathways





(A) Possible reaction pathways for the reaction of (N-DMBI-H), **IaH**, and an acceptor to form **Ia** $^{\star}$ ,  $A^{\leftarrow}$ , and H<sub>2</sub> and proceeding via an initial hydride transfer step.

(B, C) Free energies (kJ mol $^{-1}$ ) from M06/6-31G(d,p)/LANL2DZ DFT calculations (CH $_2$ Cl $_2$ ) for (B) A = 2CN-BDOPV, **2** (where the reaction does not proceed substantially beyond the first step) and (C) A = 2CN-NDI, **3b** (where  $la^+$  and  $3b^-$  are the only products observed). Note that overall  $\Delta G^0$  values for the dark purple and blue pathways are double those for the dark purple and red pathways since twice as many DH and A molecules react in the former. The activation barriers,  $\Delta G^i$ , are estimated from the experimental rate constants in Table 2 using the Eyring equation, assuming the initial hydride transfer to be rate determining.





#### TABLES, TABLE TITLES ETC.

Table 1. Electron-, Hydrogen-, and Hydride-Accepting Abilities of Acceptors Studied in This Work

Acceptor, A	Electrochemistry		DFT Calculations		
	E <sub>1/2</sub> (A <sup>0/•-</sup> ) vs. FeCp <sub>2</sub> <sup>+/0</sup> / V <sup>a</sup>	$\Delta G^{0_3b}$ / kJ mol <sup>-1</sup>	$\Delta G^{0}_{3}^{c}$ / kJ mol <sup>-1</sup>	$\Delta G^{0_4 d}$ / kJ mol <sup>-1</sup>	$\Delta G^{0}_{5}^{e}$ / kJ mol <sup>-1</sup>
1, PCBM <sup>f</sup>	-1.07 <sup>9</sup>	+83.9	+324.5 (+97.3)	+141.5 (+139.8)	+249.1 (+20.6)
2, 2CN-BDOPV	-0.58	+43.4	+246.2 (+36.4)	+112.6 (+101.2)	+140.2 (-84.2)
<b>3a</b> , NDI	-1.10	+93.6	+345.6 (+96.7)	+167.5 (+158.7)	+297.8 (+44.8)
<b>3b</b> , 2CN-NDI	-0.54	+39.6	+255.4 (+30.6)	+122.5 (+124.7)	+196.3 (-28.4)
<b>3c</b> , (CN-NDI) <sub>2</sub>	-0.72	+56.9	+248.1 (+41.9)	+124.1 (+130.4)	+196.9 (-7.7)
4a, PDI	-1.08	+91.7	+317.2 (+88.6)	+153.5 (+147.0)	+264.7 (+30.2)
4b, 2CN-PDI	-0.66	+51.1	+253.2 (+40.3)	+145.2 (+145.6)	+193.5 (-22.8)
4c, 2Br-PDI	-0.70	+55.0	+297.0 (+75.9)	+9.1 (+158.6) <sup>9</sup>	+247.0 (+20.5) <sup>9</sup>
<b>5</b> , TIPSp	-1.45 <sup>h</sup>	+127.4	+368.8 (+125.3)	+62.1 (i)	+246.8 (i)

<sup>&</sup>lt;sup>a</sup>In 0.1 M <sup>n</sup>Bu<sub>4</sub>NPF<sub>6</sub> / CH<sub>2</sub>Cl<sub>2</sub>.

 $^{b}\Delta G^{0}$  for reaction 3 (electron transfer) in solution at 298 K estimated as  $\Delta G^{0}_{3} = -F[(E_{1/2}(A^{0'\bullet}) - E_{ox}(IaH^{\bullet+/0})]$  where F is the Faraday constant and  $E_{ox}(IaH^{\bullet+/0}) = ca. -0.13 \text{ V}$  vs.  $FeCp_{2}^{*/0}$  in 0.1 M  $^{n}Bu_{4}NPF_{6}$  / THF.

 $^{c,d,e}\Delta G^0$  at 298 K for reactions in the gas phase (CH $_2$ Cl $_2$  in parentheses) represented by eq 3, 4, and 5, respectively at the M06/6-31G(d,p)/LANL2DZ level. For H $^{\bullet}$  and H $^{-}$  transfers, values correspond to the formation of the most stable isomer of AH $^{\bullet}$  or AH $^{-}$  (see Table S3 for values for other isomers and Figure S11 for structures). Note that solvation stabilizes the ionic products of electron or H $^{-}$  transfers more strongly than the neutral reactants or the products of H $^{\bullet}$  transfer, and thus the solution values of  $\Delta G^0_3$  and  $\Delta G^0_5$  are found to be considerably less endergonic; however, trends are generally similar (e.g., **3b** exhibits similar  $\Delta G^0_3$  and  $\Delta G^0_4$  values to **2** in both gas-phase and solvent, and a considerably less exergonic value of  $\Delta G^0_5$  in both the gas phase and solvent). DFT values are for  $C_{\infty}$  rather than PCBM due to the very large number of isomers possible for PCBM-H $^{\bullet}$  and PCBM-H $^{\bullet}$ .

 $^{9}$ Addition of H $^{-}$  and H $^{\bullet}$  is calculated to be more favorable for another isomer, but in solvent the C–Br bonds of those isomers dissociate; the values given here refer to the most stable isomer that does *not* dissociate.

Values in the solvent dielectric not given since DFT minimizations of the corresponding AH\* and AH\* structures in dielectric did not successfully converge.

Table 2. Rate Constants and Kinetic Isotope Effects for Reactions of Acceptors with N-DMBI-H and N-DMBI-D

А	$k_{\rm H}^{\rm a}$ / ${\rm M}^{\rm -1}$ min $^{\rm -1}$	$k_{\rm H}$ / $k_{\rm D}^{\rm b}$
1, PCBM	0.48 <sup>c</sup>	8.6ª
2, 2CN-BDOPV <sup>d</sup>	27000	5.1
<b>3a</b> , NDI	< 0.01	е
<b>3b</b> , 2CN-NDI	34.6	5.8
3c, (CN-NDI) <sub>2</sub>	2.2	5.3
<b>4a</b> , PDI	< 0.01	е
<b>4b</b> , 2CN-PDI	2.5	5.1
<b>4c</b> , 2Br-PDI	< 0.01	е
<b>5</b> , TIPSp	f	f

<sup>&</sup>lt;sup>a</sup>Rate constants for the room temperature reaction of **IaH** with A in chlorobenzene, as determined by fitting time-dependent vis.-NIR data to eq. 8 or (for **2**) eq. 9.

<sup>f</sup>No reaction observed.

<sup>&</sup>lt;sup>h</sup>Values in THF from Ref. 35.

 $<sup>^{</sup>b}$ KIE using  $k_{H}$  values and values of  $k_{D}$  obtained under the same conditions with **IaD** in place of **IaH**.

Data from ref. 29

<sup>&</sup>lt;sup>d</sup>Data for **2** correspond to formation of AH<sup>-</sup>, whereas the other acceptors form A\*-.

<sup>&</sup>lt;sup>e</sup>Reliable values of  $k_H$  and  $k_D$  could not be obtained due to extremely sluggish reactions; values of  $k_H$  are estimated upper limits.